Polyunsaturation in Lipid Membranes: Dynamic Properties and Lateral Pressure Profiles

Samuli Ollila,[†,‡] Marja T. Hyvönen,[†,§] and Ilpo Vattulainen*[,†,‡,||]

Laboratory of Physics and Helsinki Institute of Physics, Helsinki University of Technology, P.O. Box 1100, FI-02015 HUT, Finland, Institute of Physics, Tampere University of Technology, P.O. Box 692, FI-33101 Tampere, Finland, Wihuri Research Institute, Kalliolinnantie 4, FI-00140 Helsinki, Finland, and Memphys—Center for Biomembrane Physics, Physics Department, University of Southern Denmark, Campusvej 55, DK-5230 Odense M, Denmark

Received: August 22, 2006; In Final Form: December 22, 2006

We elucidate the influence of unsaturation on single-component membrane properties, focusing on their dynamical aspects and lateral pressure profiles across the membrane. To this end, we employ atomistic molecular dynamics simulations to study five different membrane systems with varying degrees of unsaturation, starting from saturated membranes and systematically increasing the level of unsaturation, ending up with a bilayer of phospholipids containing the docosahexaenoic acid. For an increasing level of unsaturation, we find considerable effects on dynamical properties, such as accelerated dynamics of the phosphocholine head groups and glycerol backbones and speeded up rotational dynamics of the lipid molecules. The lateral pressure profile is found to be altered by the degree of unsaturation. For an increasing number of double bonds, the peak in the middle of the bilayer decreases. This is compensated for by changes in the membrane−water interface region in terms of increasing peak heights of the lateral pressure profile. Implications of the findings are briefly discussed.

I. Introduction

The level of unsaturation is a strictly regulated property of all biological membranes, including cell membranes as well as intracellular specialized membranes. Unsaturated lipids are known to play a significant role in membranes, the topical and highly prominent example being the importance of polyunsaturated lipids such as those containing docosahexaenoic acid (DHA); see refs 1−4 and references therein. The lipids containing DHA have been suggested, for example, to modulate the membrane elastic stress and thereby influence the functionality of integral membrane proteins.[5] Long-chain ω-3-polyunsaturated fatty acids are also known to induce various health benefits in terms of preventing cancer and heart diseases, among others.[6]

Nowadays, double bonds are known to affect various structural membrane properties such as the area per lipid and the ordering of the acyl chains.[3,7] Yet it is evident that the ideas of the role of double bonds have changed over time as more data and more qualified methodology has become available. For instance, originally double bonds were considered as rigidifying structures in membranes due to the natural rigidity of a cis type double bond,[8,9] whereas recent studies have revealed unsaturated hydrocarbon chains to be remarkably flexible due to extraordinary isomerization of the single bonds neighboring the double bonds.[4,7,10,11] This recent progress also highlights the fact that, in contrast to the structural properties of unsaturated membranes, much less attention has been paid to understand the influence of double bonds on the dynamic properties of lipids. These effects are discussed in more detail in this article.

An especially interesting and poorly understood property of lipid membranes is the distribution of local pressure inside a bilayer, the so-called lateral pressure profile. The lateral pressure profile is related to many important macroscopic and measurable quantities, such as surface tension, surface free energy, and spontaneous curvature.[12] Furthermore, Cantor has rather recently proposed an interesting idea that changes in the lateral pressure profile may affect the functionality of mechanosensitive proteins in cell membranes,[13] which could explain, for example, the action of general anesthetics[14,15] and the coupling between protein functionality and lipid content.[14,16] It is noteworthy that Cantor's mean-field calculations[14] and atomic-scale molecular dynamics simulations of Carrillo-Tripp and Feller[17] have suggested that double bonds shift repulsive pressure from the middle of the membrane toward the interfacial region. This change has been suggested to lead to the observed increase in rhodopsin activity due to polyunsaturated lipids.[14] Interestingly, the same idea concerning the dependence of rhodopsin activity on unsaturation level has been presented earlier by Brown et al.[18−20] who discussed the role of curvature stress, which in turn is related to the lateral pressure profile and the elasticity of a membrane.

Despite the rather substantial number of studies on unsaturated membranes, it is evident that not even the recent findings do fully explain the functional properties of double bonds in membranes. Of particular interest would be to clarify the interplay between double bonds, lateral pressure, and the dynamics of membranes for varying degrees of unsaturation. That would also render the understanding of protein functionality in unsaturated membranes more comprehensible.

In this work, we present a thorough systematic analysis of unsaturated lipid membranes studied through atomic-scale molecular dynamics simulations, focusing on the dynamics and the lateral pressure profiles. Starting from saturated lipids, we systematically increase the level of unsaturation and end up with

* Author to whom correspondence should be addressed. E-mail: Ilpo.Vattulainen@csc.fi.
† Helsinki University of Technology.
‡ Tampere University of Technology.
§ Wihuri Research Institute.
|| University of Southern Denmark.

10.1021/jp065424f CCC: $37.00
Published on Web 03/03/2007

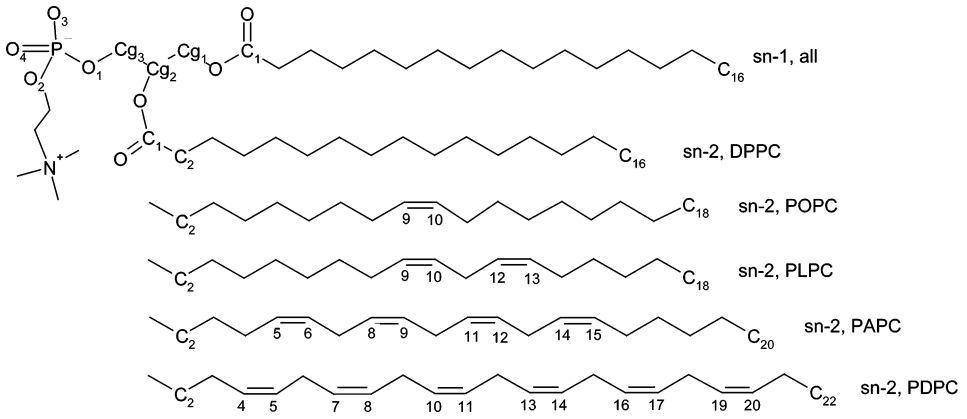

Figure 1. Structures of lipids used in bilayer simulations.

lipids containing DHA; see Figure 1. More specifically, we keep the *sn*−1 chain as well as the glycerol backbone and phosphocholine head group fixed and vary the *sn*−2 chain by considering palmitoyl, oleoyl, linoleoyl, arachidonoyl, and docosahexaenoyl chains. In this fashion, we have analyzed single-component membranes comprised of 1,2-dipalmitoyl-*sn*-glycero-3-phosphatidylcholine (DPPC), 1-palmitoyl-2-oleoyl-*sn*-glycero-3-phosphatidylcholine (POPC), 1-palmitoyl-2-linoleoyl-*sn*-glycero-3-phosphatidylcholine (PLPC), 1-palmitoyl-2-arachidonoyl-*sn*-glycero-3-phosphatidylcholine (PAPC), and 1-palmitoyl-2-docosahexaenoyl-*sn*-glycero-3-phosphatidylcholine (PDPC) lipids, as the number of double bonds in the *sn*−2 chain is increased systematically from zero to six.

The simulation data indicates that an increasing level of unsaturation leads to major changes in structural properties, such as increased area per lipid and conformationally less ordered chains. Similarly, for an increasing degree of unsaturation, we find considerable effects on dynamic properties, such as accelerated dynamics of the phosphocholine head groups and glycerol backbones and speeded up rotational dynamics of the lipid molecules. The lateral diffusion rate of the lipids studied, however, seems to be rather insensitive to the unsaturation level. In addition, we have found that the lateral pressure profile of a saturated DPPC bilayer is characterized by a repulsive peak in the middle of the membrane. For an increasing number of double bonds, the peak in the middle decreases, rendering the profile smoother in the middle of the membrane, while both positive and negative peaks at the membrane−water interface region increase in size. Implications of our findings are briefly discussed at the end of this article.

II. Methods

A. Force Field Parameters. The force field parameters employed in this work are based on a recent study by Bachar et al.[21] They adapted the force field parameters for DPPC[22] and POPC[23] to construct a force field for PLPC. For the double bond region they calculated dihedral angle parameters using ab initio techniques such that the single bonds next to the outermost double bonds as well as the bonds between double bonds are in accordance with skew$^+$ and skew$^-$ states. Further details of these potentials can be found from ref 21.

We used the PLPC force field in our work by varying the number of double bonds in the *sn*−2 hydrocarbon chain. The force field for POPC, available at http://moose.bio.ucalgary.ca/index.php?page=Downloads, was also updated such that the dihedral potentials near double bonds were in line with the ab initio calculations of Bachar et al. Other parts of the model were kept unchanged. The force field, simulation details, and some results of DPPC and PLPC have already been discussed elsewhere.[24−30]

B. Initial Structures. The initial structure for the PLPC bilayer was taken from simulations by Bachar and co-workers,[21] available at http://moose.bio.ucalgary.ca/index.php?page=Downloads. The system was comprised of 128 PLPC and 2453 water molecules. We modified the system by increasing the water/lipid ratio to 28.6 by adding 1202 water molecules to the system. Having done this, we are confident that the bilayer is fully hydrated.

The initial structure for a POPC bilayer structure was taken from the final configuration of our previous work discussed in ref 31. To construct an initial structure for a PAPC bilayer, the structure of the PLPC lipid bilayer was taken, and the two CH_2 groups were added to the *sn*−2 chain. After that, to ensure enough space for the equilibration of the system, the upper and lower monolayers were moved apart by approximately 0.5 nm. The structure was also slightly loosened in the plane of the membrane. The PDPC structure was constructed in a similar way using PAPC as a template. In all cases, the energy of the membrane systems was minimized using the steepest descent method.

C. Simulation Details. Molecular dynamics simulations were run by the GROMACS 3.1.4 simulation package.[32−34] The simulations were performed in the NPT ensemble at 1 bar and 310 K for the unsaturated systems (POPC, PLPC, PAPC, and PDPC), and at 323 K for DPPC. These temperatures are above the main transition temperatures of given lipids; thus the systems were in the fluid (liquid-disordered) phase. The simulations were carried out with the Berendsen thermostat and barostat[35] until the system had equilibrated. After equilibration the Nosé−Hoover temperature coupling[36,37] and Parrinello−Rahman pressure coupling[38,39] were applied. The coupling constant used for pressure was $\tau_p = 1.0$ ps, and for temperature $\tau_t = 0.1$ ps. The lipid bilayer and water were separately coupled to the heat bath, and the semi-isotropic pressure coupling was applied separately in the *xy*-direction (bilayer plane) and the *z*-direction (bilayer normal). The cutoff radius for van der Waals interactions was chosen as 1.0 nm. Particle mesh Ewald (PME) summations[40] were applied for long-range electrostatic interactions with a grid spacing of 0.12 nm, and a cutoff radius of 1.0 nm was employed for real space summation. In previous studies, PME has been shown to do well in membrane simulations.[25,26] The neighbor list update was performed every 10 steps. The time step was 2 fs, using LINCS[41] to constrain all bond lengths of lipids, whereas the SETTLE[42] algorithm was used for the SPC water.[43] The data saving frequency was 0.1 ps^{-1}. In total the systems were

simulated for 50.0 ns, of which the first 10.0 ns were regarded as an equilibration period and not included in analysis.

Below we compare the results of the unsaturated systems to those of a fully saturated DPPC bilayer. The simulation details and some results of the DPPC simulation study have been described elsewhere.[24−27] For this work, we have extended the analysis of the DPPC bilayer, especially in the case of lipid dynamics and the lateral pressure profile.

D. Lateral Pressure Profile. The local pressure for a system consisting of pointwise particles with *m*-body potentials can be defined using the local stress tensor

$$P = -\sigma_K - \sigma_C \tag{1}$$

The kinetic contribution of the local stress tensor σ_K is defined as[44]

$$\sigma_K^{\alpha\beta}(\mathbf{R}, t) = -\sum_i m_i v_i^\alpha v_i^\beta \delta(\mathbf{R} - \mathbf{r}_i) \tag{2}$$

where m_i, v_i, and $\mathbf{r}_i$ refer to the mass, velocity, and location of atom *i*. The definition of the configurational component of the local stress tensor σ_C for the *m*-body potential U^m is[44,45]

$$[\sigma_C^{\alpha\beta}(\mathbf{R}, t)]^{(m)} = \frac{1}{m}\Sigma_{\langle j\rangle}\Sigma_{\langle k,l\rangle}(\nabla_{j_k}^\alpha U^m - \nabla_{j_l}^\alpha U^m)\oint_{C_{jljk}} dl^\beta\, \delta(\mathbf{R} - \mathbf{l}) \tag{3}$$

where C_{jljk} is a contour from the particle j_l to the particle j_k, $\langle j\rangle$ stands for a summation over all *m*-clusters in the system, and $\langle k, l\rangle$ describes summation over all possible pairs of particles within a given *m*-cluster.

The lateral pressure profile $\pi(z)$ is then defined as a difference between the normal and the lateral components of the pressure tensor, that is, $P_N = P_{zz}$ and $P_L = (P_{xx} + P_{yy})/2$

$$\pi(z) = P_L - P_N \tag{4}$$

Qualitatively, this means that a bilayer tends to expand along the membrane plane (*xy*) with positive $\pi(z)$ and contract with negative $\pi(z)$.

The lateral pressure profile calculation is implemented to lipid bilayers by dividing the system into thin slices and calculating the local pressure tensor in each slice.[46−48] The discretization of eqs 2 and 3 leads now to the equation used in the calculations

$$\mathbf{P}^{\alpha\beta}(\mathbf{R}, t) = \Sigma_{i\in\text{slice}}\, m_i v_i^\alpha v_i^\beta + \frac{1}{mV_{\delta z}}\Sigma_{\langle j\rangle}\Sigma_{\langle k,l\rangle}(\nabla_{j_k}^\alpha U^m - \nabla_{j_l}^\alpha U^m) r_{j_k j_l}^\beta f(z_{j_k}, z_{j_l}, z_s) \tag{5}$$

where $f(z_{j_k}, z_{j_l}, z_s) = 0$ if particles are on the same side of the slice, $f(z_{j_k}, z_{j_l}, z_s) = 1$ if both particles are inside the slice, $f(z_{j_k}, z_{j_l}, z_s) = (\delta_z/|z_{j_k} - z_{j_l}|)$ if particles are on different sides of the slice, and $f(z_{j_k}, z_{j_l}, z_s) = (d_z/|z_{j_k} - z_{j_l}|)$ if only one of the particles is inside the slice. Here d_z is the distance between the particle inside the slice and the wall of the slice between the two particles, and δ_z is the thickness of the slice. The $V_\delta z$ is the volume of the slice.

Here, let us briefly comment on the chosen contour. The definition for local pressure presented above is actually unambigous due to the arbitrary contour in eq 3.[44] In practice, there are two feasible contours that can be employed. In the most intuitive and the most generally employed case, one uses the Irving−Kirkwood contour,[49,50] which goes directly from the particle j_l to j_k. A recent study by Morante et al.[51] supports the choice of this contour, too. It allows one to use eq 5, but then the range of interactions has to be finite. In practice, this implies that electrostatic interactions have to be truncated at some cutoff distance r_{cut}. In contrast, if one preferred to employ Ewald-type descriptions for long-range interactions, then the approach in eq 5 could not be used to calculate the local pressure contribution from the reciprocal space part of the Ewald sum.[46,48] Recently, Sonne et al.[48] showed that this contribution can be included using the Harasima contour.[52] Through comparison of different techniques, they concluded that the Irving−Kirkwood contour with truncation and the Harasima contour with PME yield qualitatively similar results provided that $r_{cut} > 1.8$ nm. Here, we have employed the Irving−Kirkwood contour together with truncation of electrostatic interactions at $r_{cut} = 2.0$ nm. Note, however, that while the determination of lateral pressure profiles was conducted by employing truncation via postanalysis, in the actual bilayer simulations the electrostatic interactions were treated by PME.

The practical implementation of calculations is made by dividing the system in 100 slices (approximately 0.07-nm-thick) perpendicular to the normal of the bilayer and then calculating the lateral pressure in each slice using eqs 4 and 5. The analysis is performed as a posttrajectory analysis exploiting the force field and saved locations and velocities. Forces arising from constraints are calculated using a general equation for constrained forces derived by Hess et al.[41] The estimation of statistical error for the lateral pressure profiles is made by calculating the error of the mean in each slice.

The method used here has been validated against the results of Lindahl and Edholm,[46] who used an essentially similar force field for DPPC and who also used the same contour together with the truncation for electrostatics during the pressure profile calculation. Our results for the lateral pressure profile of DPPC were found to be essentially identical.

III. Results and Discussion

A. Structural Properties. Structural properties of unsaturated systems have already been discussed in several simulation and experimental studies. We have found it essential to return to the subject due to the lack of systematic studies considering the level of unsaturation. Here we systematically vary the number of double bonds in the *sn*−2 tail by starting from a saturated palmitoyl chain and ending up in the maximally unsaturated docosahexaenoyl chain. In this fashion, we avoid potential problems due to varying force fields and simulation conditions that might hamper systematic comparison. Structural characterization serves also as a basis for the interpretation of the dynamic properties as well as the lateral pressure profiles.

1. Equilibration and Phase Behavior. As a common practice in simulations of lipid membranes (in the absence of salt), systems are considered to have achieved equilibrium when simulation box dimensions are not drifting. This condition was achieved after 10 ns for POPC, PLPC, PAPC, and PDPC (data not shown). Thereby, all results below have been analyzed over the interval of 10−50 ns of simulation time. For the DPPC bilayer, the analysis is performed over the period of 20−100 ns, which has been analyzed already in earlier studies.[24−27]

For the average area per lipid, we found 0.65 ± 0.01 nm^2 for DPPC, 0.68 ± 0.01 nm^2 for POPC, 0.69 ± 0.01 nm^2 for PLPC, 0.70 ± 0.01 nm^2 for PAPC, and 0.71 ± 0.01 nm^2 for PDPC. As a reminder, DPPC was studied at 323 K and the other systems at 310 K. The results are in good agreement with experiments. For DPPC, Nagle and Tristram-Nagle have reported a value of 0.64 nm^2 at 323 K.[53] For POPC, Kučerka et

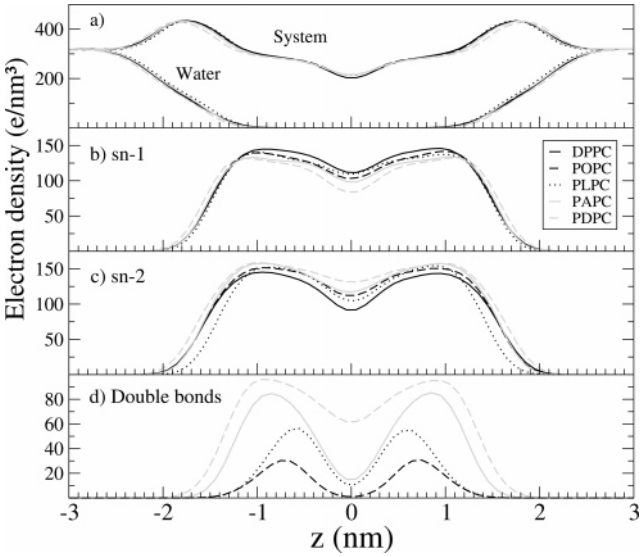

Figure 2. Electron density profiles across the bilayer for (A) the whole system together with the profile for water, (B) *sn*-1 chains, (C) *sn*-2 chains, and (D) double bonds.

al.[54] have found an area of 0.68 nm^2 at 303 K. The simulation results are also in line with the suggested trends based on various experiments:[3] The addition of first and second double bonds clearly increases the area per molecule, but additional double bonds do not seem to have remarkable effect. Additionally, although areas per lipid in monolayers and bilayers are not directly comparable, the simulation-based areas per lipid for POPC, PLPC, and PAPC are remarkably close to the respective measured values for corresponding monolayers: 0.658, 0.677, and 0.700 nm^2 (measured at 40 dynes/cm).[55] Further, our simulations reproduce the experimentally observed increase in the area per lipid from oleoyl-containing PC to arachidonoyl- or docosahexaenoyl-containing PC.[56]

Data for two-dimensional radial distribution functions of the lipid center of mass positions (not shown) indicated clearly that all bilayer systems were in the liquid-disordered phase, as expected.

2. Profiles across Bilayer and Interdigitation. In Figure 2 are shown the total electron densities of the DPPC, POPC, PLPC, PAPC, and PDPC bilayers across the bilayer, together with the separate partial densities of *sn*-1 and *sn*-2 chains and water layers together with the double bonds.

Distances between the main peaks in the total electron density profile, used generally as a measure of bilayer thickness, were for DPPC, POPC, PLPC, PAPC, and PDPC bilayers 3.6, 3.4, 3.5, 3.5, and 3.8 nm, in respective order. The experimentally determined value for the thickness of the DPPC bilayer is 3.83 nm,[53] which is in good agreement with our result. Our results for the thickness of PAPC and PDPC show also good agreement with the very recent small-angle X-ray diffraction study reporting a thickness of 3.5 nm for PAPC and 3.6 nm for PDPC.[57]

Membrane thickness does not seem to have any clear trend with regard to an increasing number of double bonds, which is probably due to the competition between various factors: Although double bonds are thought to increase the amount of tilted conformations, thereby reducing thickness, the length of the *sn*-2 chain is increasing at the same time counteracting the effects of double bonds themselves. A report of Eldho et al.[4] presents electron density curves of the DHA-containing SDPC and some other less unsaturated lipids and ends up with a conclusion that the most prominent feature in a comparison is, if the profiles are arbitrarily normalized to the same peak-to-trough extent, the broader and more shallow methyl trough region in the DHA-containing bilayer. We observe this feature in our data too, which Eldho et al. interpreted to indicate a higher density of saturated stearic acid in the bilayer center. Rajamoorthi et al.[57] interpret their very recent X-ray data for PAPC and PDPC in a similar way, suggesting that in the more unsaturated systems the saturated *sn*-1 chain would be shifted toward the membrane center. However, despite the qualitative similarity of the total electron density curves and the even quantitative agreement of membrane thickness, our simulation data would suggest the contrary: The more unsaturated the membrane, the less the saturated *sn*-1 chain appears in the membrane center; see Figure 2B. It is interesting to note, however, that if we compare just POPC and PLPC systems having *sn*-2 chains of equal lengths in carbon segments, then the density profiles of the *sn*-1 and *sn*-2 chains reproduce qualitatively the findings of the study of Eldho et al.[4]

The investigation of partial density profiles reveals also that water molecules penetrate down to the carbonyl group region (carbonyl profiles not shown), correlating with the thickness of the bilayers. Interestingly, in each system water seems to be in contact also with the hydrocarbon segments of the chains, and the probability for the contacts between water molecules and double bonds is apparently increasing with unsaturation. Unsaturared lipids are considered more susceptiple to lipid peroxidation than saturated lipids.[58] This phenomenon could be explained by the increased probability of contacts observed here. Hypothetically, increased unsaturation could ease up the entering of water-soluble oxidants to the membrane and increase the probability for their contacts with double bonds, the commonly suggested site for the beginning of membrane degrading chain reaction of oxidation.[58]

We also calculated the amount of water molecules inside bilayers, where they reside merely transiently. It can be concluded that there is more water inside a bilayer in the PAPC and PDPC bilayers than in the PLPC and POPC bilayers (data not shown). This is in agreement with the experimentally observed increase of the amount of water inside a bilayer,[3,59] when the number of double bonds is increased. As for the dynamics of water molecules in terms of permeation, during the 50 ns simulations we found only 4, 2, 7, and 6 water molecules to go through the membrane in the POPC, PLPC, PAPC, and PDPC systems, respectively. These numbers are statistically clearly too insignificant to draw any conclusions of the permeation process. After all, water molecules migrate inside bilayers relatively rarely as compared with the time scales of our present simulations. More careful studies of water inside a bilayer are therefore beyond the scope of this work.

To gain insight into the importance of interdigitation in lateral diffusion and lateral pressure profiles discussed later in this work, we quantify interdigitation as follows.[24,28] For each lipid molecule at every moment, we find its minimum and maximum *z*-coordinate, defined by the van der Waals radii of its atoms. The lipid molecule is considered to cover the whole regime between these points. The final profile is constructed by averaging over all configurations and plotting the number of the lipids as a function of the distance from the bilayer center; see Figure 3. In this fashion, one is able to study how lipid molecules in one leaflet extend to the opposite one.

The results in Figure 3 show that the interdigitation in the studied membranes is significant, but the differences between the different membranes are minor. Interdigitation in the saturated *sn*-1 chain follows the order (from largest to smallest) PLPC > DPPC > POPC > PAPC > PDPC, while in the

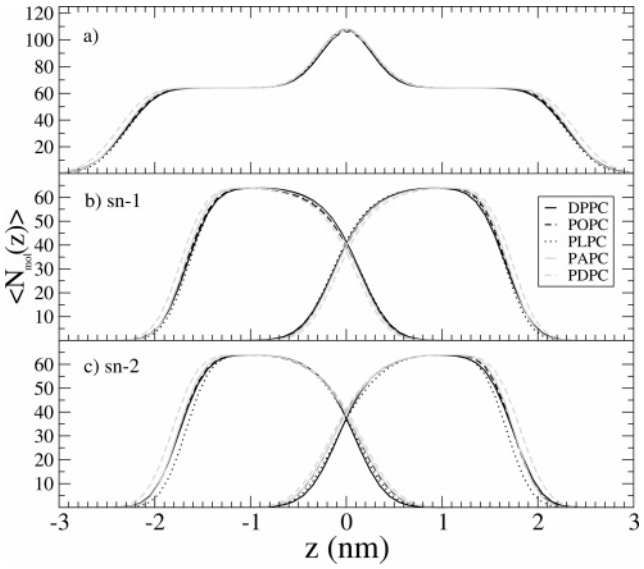

Figure 3. Average number of lipid molecules as function of distance from bilayer center along the bilayer normal. Results are shown for (A) the whole system, (B) the *sn*-1 chain, and (C) the *sn*-2 chain. For comparison, the number of lipids in each leaflet is 64.

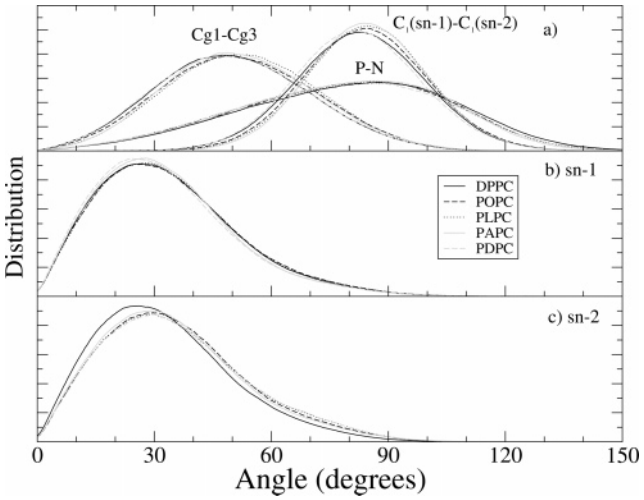

Figure 4. Angular distributions of several vectors characterizing molecular orientations. (A) Head group (P−N vector) and glycerol (Cg1−Cg3) backbone vectors together with the vectors between first carbons of *sn*-2 and *sn*-1 chains (C1(*sn*-1)−C1(*sn*-2)) with respect to the outward bilayer normal. (B) Vector from the first to the last carbon of the *sn*-1 chain with respect to the inward bilayer normal. (C) As in part B, but for the *sn*-2 chain.

unsaturated *sn*−2 chain the order is essentially opposite PDPC > PAPC > POPC > PLPC > DPPC. When it comes to the total interdigitation, it is to some extent enhanced for increasing unsaturation, though the differences are indeed minor.

3. Orientation of the Head Group, Glycerol Backbone, and Hydrocarbon Chains. The angular distributions of various vectors describing the overall structure of the studied unsaturated molecules have been calculated with respect to the bilayer normal and are shown in Figure 4. The broad distributions show that the average orientation angle of the phosphorus−nitrogen (P−N) vector with respect to the outward bilayer normal is practically similar, 78° ± 1°, in all five systems. This agrees well with the experimental estimate of, for instance, 72° by Akutsu and Nagamori.[60] This leads to the conclusion that head groups lie, on average, almost in parallel to the bilayer surface and that unsaturation has only a minor effect on the orientation of the head group. The widths of the distributions demonstrate, however, that the membrane−water interface is subject to considerable fluctuations and rather rough, as the head groups may occasionally point directly toward the water phase and next almost toward the interior of the bilayer.

Figure 4 shows also the angular distributions of the glycerol backbone vector, determined as a vector from the *sn*-1 carbon to the *sn*-3 carbon of the glycerol group. Again there is no significant difference between the different lipids, as the most prevailing orientation angle of the glycerol backbone in the different systems is 48° ± 3°. The angular distribution of the vector from the first carbon of the *sn*-1 chain to the first carbon of the *sn*-2 chain presents also no significant differences between the bilayer systems, showing only that in all systems this vector lies on average almost in parallel to the bilayer surface making the chains to start approximately from the same height. Hence, these distributions do not reveal significant differences in the head group and interfacial regions between the different unsaturated bilayers. The widths of the distributions demonstrate the dynamic nature of the interface.

Figures 4B and 4C depict the angular distributions of the vectors from the first to the last carbons of the hydrocarbon chains and are shown with respect to the inward normal of the bilayer. The most prevailing angles for the *sn*-1 chains of the DPPC, POPC, PLPC, PAPC, and PDPC bilayers are 27°, 25°, 28°, 28° and 24°, respectively, and for the *sn*-2 chain 26°, 30°, 30°, 30°, and 30°. These values are in line with suggestions based on fluorescence emission experiments:[59,61,62] Addition of fthe irst double bond increases the tilt angle, but addition of more double bonds has a minor effect. However, since the observed changes are small, conclusions must be drawn with care as well.

4. Chain Structures. We have determined the deuterium order parameter

$$S_{CD} = \frac{1}{2}\langle 3\cos^2\theta - 1\rangle \qquad (6)$$

where θ is the angle between the bilayer normal and the C−H bond vector and the brackets denote an average over all lipids and different times. To calculate deuterium order parameters from eq 6, the positions of hydrogen atoms had to be included in the simulation trajectories of the system, which was performed by calculating the positions on the basis of the orientation of carbon chains and exploiting tetrahedral symmetry at given sites. A similar approach has been used elsewhere.[27] Figure 5 shows the order parameters of the *sn*-1 and *sn*-2 chains of DPPC, POPC, PLPC, PAPC, and PDPC bilayers. For clarity's sake, error bounds have been calculated for all carbons but plotted only for selected ones.

Order parameters for the *sn*-1 chains of the bilayers with a different level of unsaturation appear to be approximately similar; see Figure 5F. The ^{2}H NMR study of Holte et al.[63] suggests that adding the second and third double bond into the *sn*-2 chain decreases the order of the *sn*-1 chain, but adding further double bonds would not cause a further decrease in ordering. Nevertheless, the observed changes in experiments are also small. Taking into account the experimental uncertainties, simulations and experiments are in good agreement. Especially in the case of the DPPC and POPC bilayers, quantitative agreement with experiments is very good.

For the PLPC bilayer there are no experimental order parameter results available, so the comparison is made mostly for the *sn*-2 linoleate chain. Here, the order parameters are measured for the isolinoleate chain of 1-palmitoyl-2-isolinoleoyl−glycero-3-phosphocholine (PiLPC),[64] in which the loca-

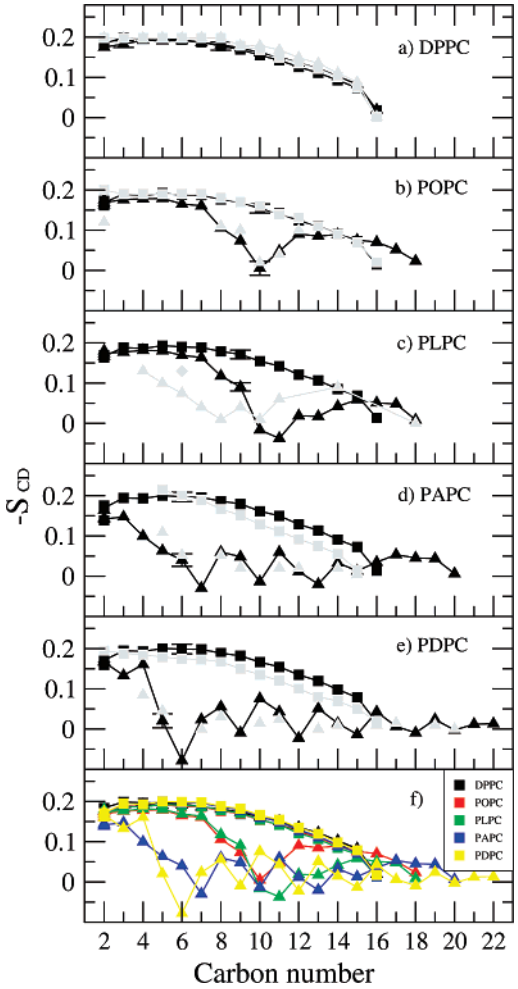

Figure 5. Order parameters for the *sn*-1 (squares) and *sn*-2 (triangles) chains of (A) DPPC, (B) POPC, (C) PLPC, (D) PAPC, and (E) PDPC. Simulation results are shown in full black, and experimental results for comparison in gray. Additionally, part F summarizes the data for all bilayers from the simulations. Experimental order parameters were chosen for comparison as follows. The order parameters for DPPC (T = 323 K) are based on studies by Petrache et al.[98] whereas the experimental S_{CD} values for PDPC and for the *sn*-1 chain of POPC (T = 310 K) are based on studies by Huber et al.[67] For the *sn*-1 chain of PDPC, the data set at 310 K is obtained by linearly interpolating between data at 303 and 323 K, whereas for the *sn*-2 chain the data at 303 K are presented.[67] Experimental values for the *sn*-2 chain of POPC are based on studies by Seelig et al.[99] A single experimental value is available also for the *sn*-2 chain of the PLPC bilayer at 313 K (diamond)[64] to compare with our simulated order parameters for PLPC. Together with PLPC, there are also experimental results for PiLPC (T = 313 K).[64] Experimental order parameters for the *sn*-1 and *sn*-2 chains of PAPC (T = 303 K) are based on quadrupole splittings measured by Rajamoorthi et al.[100] For the *sn*-1 chain the monotonic decrease through the acyl chain is expected. For the *sn*-2 chain, values are fitted such that the agreement is as good as possible.

tion of double bonds is shifted three carbons toward the glycerol backbone. If this shift is taken into account in the comparison together with the fact that the experimental order parameters are absolute values, then the comparison of the profile shapes suggests very good agreement between the simulations and experiments due to two double bonds. This is further supported by the single measurement in the experiments of Baenziger et al.[64] for carbon C6 of the *sn*-2 chain of PLPC, Figure 5C, which agrees with our simulation-based value. Order parameters of the *sn*-1 chain of the PLPC bilayer agree well with simulations by Bachar et al.[21]

In the PAPC and PDPC bilayers, the *sn*-1 chains seem to be more ordered in our simulations than in experiments. However, the assignment of the order parameter from ^{2}H NMR experiments with perdeuterated acyl chains is not segment-specific but assumes monotonically decreasing order toward the chain ends. If this assumption were not done for experimental values, then the experimental order parameter profile would likely be more similar to ours in the beginning of the chains. What is more, in addition to the results presented in Figure 5, the experimental results for the sn-1 chain order parameters of PAPC[65] and PDPC[66] agree with our results. Qualitatively the difference between the *sn*-1 chains of PAPC and PDPC in our simulations is similar to the ^{2}H NMR study[57]of Rajamoorthi et al.: In the same absolute temperatures the order parameters of the *sn*-1 chains of PAPC are closer to zero than those of PDPC.

It is noteworthy that we find nearly identical, almost zero, order parameter values in the last segments of the chains in each bilayer, indicating almost full orientational freedom of the methyl segment in the bilayer center. This is in full agreement with experimental findings, wherever comparison is possible.

As the number of double bonds in the *sn*−2 chain increases, the order parameters at the double bond regions apparently approach zero indicating lower order. Interestingly, Eldho et al.[4] mention in their deuterium NMR study that the order parameters of docosahexaenoyl and docosapentaenoyl chains (in the *sn*-2 position) for carbons in double bonds show higher order at the first carbon in the bond relative to the second. A similar feature is mostly observed also in the order parameter profiles of arachidonoyl and docosahexaenoyl chains as calculated from our simulations. However, the order parameter profile measured for the *sn*-2 docosahexaenoyl chain by Huber et al. for PDPC is much smoother.[67]

In all, the comparison of our simulation-based order parameters with corresponding experimental results shows good agreement, even at a quantitative level, especially taking into account the apparent differences in order parameters between different experimental systems.

The fractions of trans/gauche$^+$/gauche$^-$ or skew$^+$/skew$^-$ states along the chains were calculated for each bond along the chain, depending on the type of the bond (data not shown). In all bonds of *sn*-1 chains the fraction of gauche states is approximately 20−25%, except for the last dihedral, where the amount increases to 30%. However, there is very little variation between different bilayers. The general amount accords with the Fourier transform infrared spectroscopy experiments for a DPPC bilayer.[68] The fraction for skew$^+$ states in *sn*-2 chains is approximately 50% as can be expected from the dihedral potential applied.[21] Trans fractions for saturated regions in *sn*-2 chains are approximately similar to those in *sn*−1 chains, except for a bond closest to the skew-type bonds. In those bonds the amounts of trans states are decreased to approximately 50−65%.

B. Dynamic Properties. *1. Lateral Diffusion.* The lateral diffusion rate of lipid molecules in the plane of the bilayer is described by the lateral diffusion coefficient. Among several experimental methods, the fluorescence recovery after photobleaching, nuclear magnetic resonance, and single-particle tracking have been perhaps the most popular techniques to consider lateral diffusion for lipid bilayers.[69]

The lateral diffusion coefficient D for single-particle motion is defined as

$$D = \lim_{t\to\infty} \frac{1}{2dt}\langle[\vec{r}(t) - \vec{r}(0)]^2\rangle \qquad (7)$$

where $d = 2$ is the dimensionality of the system and $\vec{r}(t)$ is the molecule's center of mass position at time t. Hence, $\langle[\vec{r}(t) - \vec{r}(0)]^2\rangle$ constitutes the mean-squared displacement (MSD) of a single tagged particle, which is then averaged over different time origins and molecules in the bilayer. Importantly, since the center of mass of individual monolayers in a membrane may drift during the simulation, there is reason to consider single-particle motion with respect to the leaflet's center of mass motion. Here, we took this effect into account in a similar fashion as in ref 25.

Having calculated the MSD as a function of time, we determined the diffusion coefficient D from the slope of the MSD over time windows of 2−3 and 5−10 ns. The studied two cases allowed us to estimate the error bounds with reasonable accuracy. The results shown below refer to the longer time scale.

Through this analysis, we found a lateral diffusion coefficient of $(12 \pm 3) \times 10^{-8}$ cm^2/s for DPPC, $(9 \pm 3) \times 10^{-8}$ cm^2/s for POPC, $(13 \pm 3) \times 10^{-8}$ cm^2/s for PLPC, $(9 \pm 3) \times 10^{-8}$cm^2/s for PAPC, and $(11 \pm 3) \times 10^{-8}$ cm^2/s for PDPC. There is reason to keep in mind that the DPPC simulations were carried out at 323 K and the others at 310 K.

The simulations indicate that the studied systems have very similar lateral diffusion coefficients as the differences are within the error bars. Therefore, the data propose that unsaturation in the *sn*-2 chain does not affect lateral diffusion rates in a significant fashion, or if it does, then there are competing mechanisms with opposing trends. For example, one is tempted to assume that increasing unsaturation increases the rate of lateral diffusion, because the area per lipid and hence also the free volume available to diffusion increases; see section III.A.1. However, since in our case the increase in unsaturation is associated to an increase in the length of the *sn*-2 chain, one might expect the increasing interdigitation to slow down diffusion (Figure 3). However, the results shown in Figure 3 indicate only minor differences in interdigitation between the studied membranes. Additionally, what might play a role in lateral diffusion is the effect of entanglements: For long enough chains, their lateral motion is slowed down since they are entangled with other chains, and this effect increases for increasing chain length. It is likely that all these processes contribute to the lateral diffusion studied here, but nevertheless, within the quality of the data, the lateral diffusion rate seems to only rather weakly depend on the unsaturation level.

As for the trend of increasing unsaturation level, comparison to previous simulations and experiments is rather difficult because, to our knowledge, there are no systematic studies available for comparison. The wide range of published values indicates some uncertainty concerning the actual diffusion rate and is likely, in part, due to different experimental techniques considering diffusion phenomena over different scales in space and time. Let us therefore concentrate on the work by Filippov et al., who have systematically used pulsed-field gradient NMR to measure lateral diffusion in several one-component systems. At 323 K, they found 14×10^{-8} cm^2/s for DPPC,[70] and at 313 K a lateral diffusion coefficient of 13.5×10^{-8} cm^2/s for POPC.[71] If one assumes the Arrhenius form to hold and uses the Arrhenius barrier of 28 kcal/mol found by Filippov et al.,[71] then one finds 12.1×10^{-8} cm^2/s for POPC at 310 K. The trend here is in reasonable agreement with our simulation results. Similarly, Vaz et al.[72] used fluorescence recovery after photobleaching and found 12.5×10^{-8} cm^2/s at 323 K for DPPC and 7×10^{-8} cm^2/s at 313 K for POPC. The trends in these results are in agreement with the simulation data, too. For DOPC, Filippov et al.[71] and Ladha et al.[73] found a slightly higher diffusion coefficient than for POPC. As the hydrocarbon chains of POPC and DOPC are almost of equal length and the average area per lipid is slightly larger for DOPC than for POPC,[54] this trend is expected and is in line with the simulation data; see above. Preliminary results of Dustman et al.[74] based on pulsed-field gradient magic-angle spinning NMR experiments have indicated an increase in the diffusion rates upon increasing unsaturation. Mitchell and Litman[59] have reported increased dynamics of the fluorescent diphenylhexatriene (DPH) probe in lipid bilayers for increasing unsaturation, but in this case one has to keep in mind that the results reflect the dynamics of the probe rather than the behavior of the unlabeled lipid molecules.[29,30] Finally, concerning previous simulations, a study by Niemela et al.[75] showed that for sphingomyelin bilayers the monounsaturated lipids expressed faster diffusion than the saturated counterpart. However, they also found that increasing chain length slowed down lateral diffusion. We come back to this issue at the end of this article.

2. Intramolecular Dynamics. The understanding of intramolecular dynamics of lipids is largely based on NMR studies, complemented by computational studies of rotational autocorrelation functions that provide related data for comparison. For this purpose, we consider here the autocorrelation functions of various vectors describing different parts of the lipid molecules: the glycerol region through the vector from the *sn*-1 to the *sn*-3 carbon, the head group region through the P−N vector, and the C−H vector of individual carbon−hydrogen bonds along the hydrocarbon chains (Figure 1). In practice, we employ the second-order reorientational autocorrelation function[27]

$$C_2(t) = \frac{1}{2}\langle 3[\vec{\mu}(t)\cdot\vec{\mu}(0)]^2 - 1\rangle \tag{8}$$

where $\vec{\mu}(t)$ is a unit vector that defines the chosen rotational mode; see above. To characterize the motion of the molecular parts, either the half-times of the decay, $t_{1/2}$, or the effective characteristic times, τ_{eff}, were determined from the autocorrelation functions. The effective characteristic time of the autocorrelation function is defined by

$$\tau_{\mathrm{eff}} = \int_0^\infty \mathrm{d}t\, \frac{C_2(t) - C_2(\infty)}{C_2(0) - C_2(\infty)} \tag{9}$$

where $C_2(\infty)$ is the plateau value of the autocorrelation function at long times and $C_2(0) = 1$ due to normalization. Equation 9 stems from the assumption that the decay of $C_2(t)$ is exponential. Here, the characteristic time is called effective because this is not the case, that is, the autocorrelation functions of the C−H vectors are not truly exponential but rather have several characteristic time scales. This has been shown rather recently in several studies,[4,76,77] which have found evidence for the idea that the decay of $C_2(t)$ follows a power law or stretched exponential, though the present view is inconclusive in the sense that both forms seem to describe the data equally well (and asymptotically one expects exponential decay for a dissipative system). Our results (not shown) support these findings. The relevance of using eq 9 therefore lies in the idea that it allows us to systematically compare the influence of double bonds on the chain dynamics between the many different lipid types. Though these results are suggestive and describe the rate of dynamics in an averaged sense, the effective correlation time grasps the essential behavior.

Figure 6A presents the data for the decay half-times for these autocorrelation functions. Figures 6B and 6C, in turn, show the

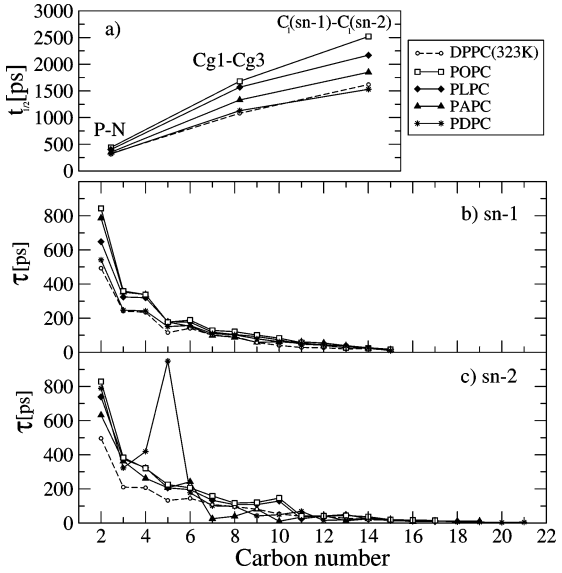

Figure 6. (A) Decay half-times for autocorrelation functions of P−N, Cg1−Cg2, and C1(*sn*-1)−C1(*sn*-2) vectors. Parts B and C show effective characteristic times for autocorrelation functions of C−H vectors along the hydrocarbon chains in different bilayers. Note that the DPPC bilayer was simulated at a higher temperature of 323 K, resulting in the more rapid dynamics seen here.

effective characteristic times for autocorrelation functions of C−H vectors in the acyl chains.

The decay half-times of the reorientational autocorrelation functions of the head group and glycerol backbone vectors together with the C1(*sn*-1)−C1(*sn*-2) vector show that in our model membranes the rotational dynamics of these vectors become faster as the number of double bonds increases from one to six. Autocorrelation functions of these various vectors would indicate the C1(*sn*-1)−C1(*sn*-2) vector to have the slowest motion of the vectors compared here. This is, however hand, natural, as the C1(*sn*-1)−C1(*sn*-2) vector lies on average in the bilayer plane (Figure 4), and the motion therefore represents roughly the rotational motion of the whole molecule, which is expected to be a slow process. It is interesting to note that although we cannot observe a significant trend in the lateral diffusion coefficients along the increasing unsaturation (see discussion above), there seems to be a clear trend of increasing rotational motion in the P−N, Cg1−Cg2, and C1(*sn*-1)−C1-(*sn*-2) vectors for increasing unsaturation.

From Figure 6 one can observe that the rotational dynamics of C−H vectors, for both chains, are considerably slower near the head group than near the bilayer center. This behavior has also been reported based on experiments for both saturated[78] and unsaturated[4,7] chains. Unsaturation does not seem to have a significant effect on the rotational dynamics of C−H vectors in the *sn*-1 chain in our simulation time scale, except for faster dynamics in the three first carbons.

The profile of the effective characteristic times for the *sn*-2 chains suggests that the rotational dynamics of the carbon segments are significantly increased after each double bond toward the methyl end. In most cases this leads to exceptionally rapid rotational motions between the double bonds, while the dynamics of the double-bonded carbons might be relatively slow. This observation is in line with various experiments.[4,7,79]

Rotational autocorrelation functions of C−H vectors can be compared with the spin lattice relaxation times from ^{2}H NMR and ^{13}C NMR experiments according to the procedure presented, e.g., in refs 4 and 76. Here we have made this comparison to ensure that our dynamics are in agreement with experimental results. We have determined the spectral densities by fitting the four exponential sums on the autocorrelation functions as in ref 4 and then applied the equations in ref 76. All available spin lattice relaxation times increase toward the end of the acyl chain.[4,57,78,80] For carbons 2−14 in the *sn*-2 chain of DPPC, spin lattice relaxation times between 0.5−1.7 and 0.02−0.1 s are obtained from ^{13}C NMR (conducted at 126 MHz, 323 K)[80] and ^{2}H NMR (54.4 MHz, 324 K)[78] experiments, respectively. In our analysis, spin lattice relaxation times have been calculated from simulation data using the same NMR frequencies as used in experiments. The experimental results are then found to be in good agreement with our results giving 0.1−1.7 and 0.003−1.4 s, in respective order. According to ^{13} C NMR (125.7 MHz, 303 K) results[4,7,81] for a bilayer containing DHA chains, the spin lattice relaxation times are approximately between 0.3 and 2 s for carbon numbers 2−17, increasing stepwise from one double bond to another toward the methyl end. According to the same studies, ^{13}C NMR spin lattice relaxation times for carbons 19−22 in the DHA chain are between 3 and 5 s. Our simulations give spin lattice relaxation times between 0.29 and 5 s for carbons 2−17, having a similar stepwise increase, and times between 9 and 22 s for carbons 19−22. In general, the qualitative and even quantitative agreement between experiments and our simulations is good.

For the purpose of completeness, we also analyzed the transition rates between gauche and trans states in the single bonds and between skew$^+$ and skew$^-$ states in the single bonds next to the double bonds (data not shown). For this purpose, due to remarkably high transition rates, each system was simulated for an extra 1 ns with a greater data saving frequency of 50 ps^{-1} to be able to determine reliable transition rates. The transition rates in the bonds of the chains range between 20 and 450 transitions per nanosecond; see below.

Transition rates for *sn*-1 chains of the unsaturated lipids do not appear to vary significantly between the different unsaturated systems. The rates increase from the beginning of the *sn*-1 chain toward their end, being approximately 35−45 ns^{-1} until the bond C12−C13, after which the rate increases to a value of 65 ns^{-1} in the bond C14−C15. In the *sn*-1 chain of the DPPC system, the behavior is similar to other systems, but the number of transitions is increased by approximately 10 ns^{-1} for each bond, probably due to the higher simulation temperature.

A similar increase of transition rates toward the bilayer center is found also in the *sn*-2 chain. The exception to this behavior concerns the transition rates for the skew-type bonds next to the double-bonded regions, where the rates are especially large, larger than 350 ns^{-1}, while in the region between the double bonds the rate is roughly twice the normal value of single bonds, i.e., approximately 100 ns^{-1}. Similar trends have been seen in CHARMM simulations of Hyvönen et al.,[11,82] though there the rates were clearly smaller than in our present simulations. These variations may be due to a different data saving frequency or differences in force fields. Interestingly, Gawrisch et al.[7] and Eldho et al.[4] have proposed that the increased flexibility in bilayers with an increasing number of double bonds may be caused by conformational freedom and structural transition rates near double bond regions. They assumed, however, that the dynamics of all skew-type bonds would be equally fast, both at the edges and inside the double bond regions. Simulation studies would suggest, though, that the profoundly high transition rate would take place only at the edges of the double bond regions, although the rate would be significantly increased also in the skew-type single bonds between the double bonds. This type of behavior would guarantee, altogether, a very flexible nature

for the highly unsaturated bilayers, especially those containing DHA, as has been suggested also based on solid-state NMR experiments.[7]

Taken together, we find good agreement with the corresponding dynamic properties in related experimental systems, whenever comparison is possible. This lays sound background for the interpretation of our other results for which experimental data does not exist, such as the lateral pressure profiles discussed below.

C. Lateral Pressure Profiles. The concept of lateral pressure profile, $\pi(z)$, arises from local forces acting inside a lipid bilayer in the direction of the membrane plane; see section II.D.

In equilibrium, to guarantee mechanical stability of the membrane, the integrated lateral pressure profile across the membrane should be zero. Yet the profile may spatially express different behaviors due to different interaction types. Traditionally three different regimes have been identified: a repulsive contribution arising from hydrophilic head groups due to electrostatic and steric interactions and hydration repulsion; an attractive contribution due to the interfacial energy between the water and the hydrocarbon phase, trying to minimize the surface area; and a repulsive contribution from the hydrophopic chains due to steric interactions.[83−85] These forces are assumed to create a nonuniform lateral component of local pressure inside a bilayer.[85,86]

Previous atomistic simulation studies[17,46−48,87] have shown that the lateral pressure profile depends on the lipid composition of the membrane and is characterized by narrow local peaks on the order of 1000 bar. Mean-field analytical predictions[14] and simulations of coarse-grained model systems[45,88] have provided support for these conclusions. On the basis of these exceptional properties, it has been suggested that the functioning of certain membrane proteins is influenced by the lateral pressure profile,[13] and it may even provide a mechanism for the action of anesthetics affecting the state of membrane proteins such as ion channels. However, the lateral pressure profile is extremely difficult to measure experimentally. To our knowledge, there is only one rather recent study[89] in which fluorescent probes were utilized to gauge the lateral pressure at several places in the hydrocarbon part of a membrane to determine the qualitative form of the pressure profile. In general, the atomic-scale molecular dynamics method seems to provide the most accurate means to elucidate lateral pressure profiles.

Here we employ the atomic-scale simulation data to systematically analyze the dependence of lateral pressure profiles on the unsaturation level. The results are presented in Figure 7. For clarity, the profiles have been smoothed by adaptive high order spline fitting[90] and averaged over the two monolayers. Original data are presented in the Supporting Information.

The lateral pressure profile found for DPPC is in good agreement with earlier atomic-scale simuations.[46,48,87] Considering the present case, the profile is most importantly characterized by the negative peak at the boundary between the water and hydrophopic phases and by the shallow peak in the middle of the bilayer. The origin of the latter is still under debate;[91] see below.

We find that the main effect of increasing the number of double bonds is the decrease of the lateral pressure in the middle of the membrane, for $|z| < 0.5$ nm. The largest difference at this region, 180 bar, is obtained between DPPC (saturated) and PDPC (six double bonds), though the effect due to increasing unsaturation seems to be most pronounced when the first two double bonds are incorporated into the *sn*-2 chain. We also find that the reduction of lateral pressure in the membrane center is

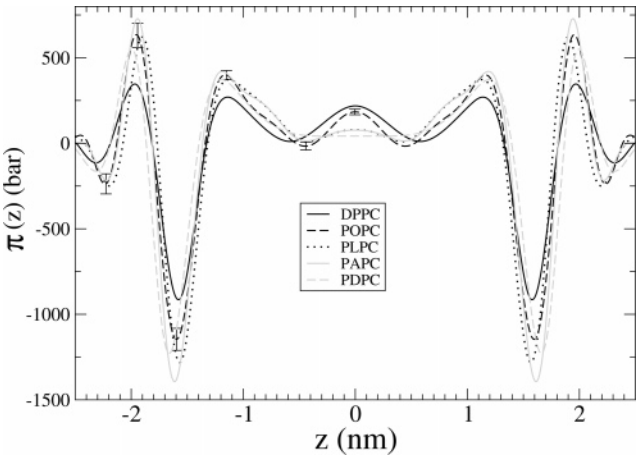

Figure 7. Lateral pressure profiles of DPPC, POPC, PLPC, PAPC, and PDPC bilayers, having zero, one, two, four, and six double bonds, in respective order. Statistical errors are presented for one leaflet of the POPC system. Error bars in the other leaflet and in other systems are similar.

partly compensated for by an increase of lateral pressure on both sides of the membrane−water interface, but these changes are not as systematic as in the middle of the bilayer.

Previously, the peak in the middle of the bilayer has been suggested to emerge from interdigitation of the two leaflets.[91] To consider this possibility, we analyzed the interdigitation in a similar manner as in ref 75 and found that the interdigitation does not significantly change when the number of double bonds is increased; see Figure 3. This result suggests that the disappearance of the peak in the membrane center in Figure 7 cannot be explained straightforwardly by interdigitation.

Carrillo-Tripp and Feller[17] have calculated lateral pressure profiles from atomistic molecular dynamics simulations for lipid bilayers having six and five double bonds in the *sn*-2 chain, with equal chain lengths (18:0−22:6n3PC and 18:0−22:5n6PC). Their main result was that the addition of a double bond increases the pressure near the interfacial region, which is in agreement with lattice thermodynamics calculations of Cantor.[14] They did not, however, observe a change in the middle of the bilayer. Furthermore, according to ref 17, the repulsive chain pressure follows the distribution of the polyunsaturated acyl chain segments. Figures 2 and 7 indicate that we find somewhat different behavior, especially in the middle of the bilayer, where the density of the unsaturated chains increases, the pressure decreases contrary to the suggestion of ref 17. We think that the reasons for these differences with respect to our work are partly methodological and subject to the lipids studied. First, the area of the bilayer was held constant during the simulations in ref 17, and this area was also identical in the simulations of the two different unsaturated bilayers (18:0−22:6n3PC and 18:0−22:5n6PC). This does not allow the system to find its equilibrium area with zero surface tension (see section III.A.1). Second, Carrillo-Tripp and Feller compared only lipids that have equal chain lengths, but a different number of double bonds. This is also the case between POPC and PLPC systems, but those include, however, only one and two double bonds and thus are not fully comparable with the systems of ref 17. In most of the systems studied here, both the number of double bonds and the chain length are varied.

The relation between the deuterium order parameter and the lateral pressure has been discussed rather recently, but no general consensus has been achieved.[16,92] Gawrisch and Holte have observed that an increase of temperature, chain length, or level of unsaturation promotes the formation of an inverse lamellar

phase and decrease lipid ordering. Thus, they have suggested that a decrease in the order of the hydrocarbon chains increases the lateral pressure in the acyl chain region.[92] From Figures 5 and 7 it can be seen that near the interfacial region the absolute value of the deuterium order parameter decreases due to double bonds, but the lateral pressure remains almost unchanged. At the same time, in the middle of the bilayer the lateral pressure decreases due to double bonds, but the deuterium order parameter is only weakly affected. Thus, our results do not suggest any clear-cut relation between the deuterium order parameter and the lateral pressure.

In fact, all of the above-mentioned results[14,16,17,92] also agree with our results, which is, however, not trivial. First, in our simulations as well as in experimental results the order remarkably decreases near the interfacial region for increasing unsaturation. On the basis of the above suggestion, the repulsive pressure is expected to increase in that region. This increase would lead to an increase in the area per lipid, which has been observed in experiments[7] and our simulations. However, the order in the middle of the bilayer is not significantly changed due to unsaturation, and thus, according to the suggestion above, the repulsive pressure in that region is expected to be approximately equal in all systems regardless of the number of double bonds. This argument leads to a conclusion that the lateral pressure in the middle of the bilayer is decreased due to polyunsaturation, because the area per molecule increases accordingly. Furthermore, the maximum in the middle of a saturated or monounsaturated membrane can be explained by reduced ordering in the middle of the membrane compared with the interfacial region. This idea is in good agreement with the suggestion of Mukhin and Baoukina[93] who have proposed that the peak in the middle of the bilayer is induced by increased configurational entropy due to the low order.

Quantitatively, the differences between the lateral pressure profiles of saturated and polyunsaturated lipid bilayers in the middle of the bilayer are approximately a few hundred bars. The change is substantial, and approximately 15% of the peak value is close to the membrane−water interface. It is likely that changes of this size may play a role in membrane protein functionality. This is substantiated by the theory of Cantor, which predicts that changes in the lateral pressure profile affect exponentially the ratio of concentrations of conformational (functional) states of mechanosensitive proteins.[13] Furthermore, it has been suggested that changes in the lateral pressure profile are involved in increasing rhodopsin activity with increasing level of unsaturation.[14,20,94] Being more specific, this proposition was first made in terms of curvature stress by Brown et al.[18−20] and later extended more explicitly by Cantor.[14] Our results support this view, because double bonds seem to systemically decrease the repulsive pressure in the middle of the bilayer. It also seems evident that the active state of rhodopsin has a larger volume than the inactive state.[95] In addition, the crystal structure of rhodopsin[96] suggests that the retinal, the origin of the activation, locates rather close to the center of the bilayer. Cholesterol, in turn, has been observed to decrease rhodopsin activity,[94] while the atomic-scale molecular dynamics calculations of several authors[17,87,97] suggest that cholesterol increases the repulsive pressure in the middle of the bilayer. These results encourage us to hypothesize that the activity of membrane proteins such as rhodopsin is affected by changes in the lateral pressure profile in the middle of the membrane. More direct studies including proteins embedded in membranes would be most welcome to validate this idea.

IV. Concluding Remarks

Here, we have employed atomistic molecular dynamics simulations to thoroughly elucidate the effects of unsaturation on lipid bilayer properties. The *sn*-1 chain in phosphatidylcholines was held fixed (palmitoyl), while the *sn*-2 chain was varied systematically by changing its unsaturation level and length. In this fashion, we analyzed single-component membranes comprised of DPPC, POPC$^{\Delta 9}$, PLPC$^{\Delta 9,12}$, PAPC$^{\Delta 5,8,11,14}$, and PDPC$^{\Delta 4,7,10,13,16,19}$. The focus of the study was on the dynamics and lateral pressure profiles and in particular on the changes in system properties as the level of unsaturation was varied systematically in a controlled manner.

First, as for structural properties, one of the most obvious effects found in the fluid (liquid-disordered) phase is the increase in the area per lipid, which is most prominent after the incorporation of the first double bond, that is, the area per lipid is increased in the POPC bilayer as compared with saturated DPPC. This results in many other structural effects in quantities such as the ordering of lipid hydrocarbon chains, membrane thickness, and density profiles across the membrane.

Recently, it has been proposed[4,5,57] that there would be an uneven distribution of density in DHA-containing bilayers as compared with less unsaturated ones: The saturated *sn*-1 chain would be displaced toward the bilayer center whereas the *sn*-2 polyunsaturated chain would be shifted toward the bilayer−water interface. This kind of conclusion cannot directly be drawn from our simulations, if the PDPC bilayer is compared with PAPC, as was done by Rajamoorthi et al.[57] However, this type of distributional difference can be interpreted to appear when comparison is made between POPC and PLPC bilayers, having chains with an equal number of carbon segments like in the comparison carried out in the study of Eldho et al.[4]

No major differences were found to appear in the orientational distributions of the head groups or vectors of the interfacial regions with respect to the bilayer plane; the head groups lie on average parallel to the membrane surface. Incorporation of double bonds into the fatty acyl chains naturally affects their structural properties. In our simulations the effects on the order parameters of the *sn*-1 chains were found to be minor, but in the case of unsaturated *sn*-2 chains the order parameters are strongly reduced locally at the regions of the double bonds. Close to the last carbon segments in the tails of the chains, the order parameter is essentially zero in all systems and for both chains indicating full orientational freedom. Overall, our simulation data for the order parameters of acyl chains are in good agreement with NMR measurements.

Second, concerning dynamics of the membranes, the lateral diffusion coefficients in the studied systems were observed to lie in the range $(9-13) \times 10^{-8}$ cm ^{2}/s, in good accordance with the few and varying experimental values available. However, as far as we know, no systematic reports appear to exist yet for the effect of unsaturation on lateral diffusion in the lipid bilayer systems. The present results seem to indicate that unsaturation plays a minor role for lateral diffusion. However, this conclusion should be taken with a grain of salt, since in the lipids considered in this work both the number of double bonds and the length of the hydrocarbon chains were varied. As the area per lipid increases for increasing unsaturation, one expects the lateral diffusion to speed up, too. However, this holds only for chains of equal length. If the length of the hydrocarbon chains increases, then entanglement effects become more prominent, and interdigitation may increase as well. These effects are expected to counter-balance the effect of increasing area per lipid and to slow down diffusion. To fully elucidate the effect

of unsaturation on lateral diffusion, further comparative studies with lipids of equal length would be most welcome. NMR, in particular, might be the method of choice to clarify this issue.

Though no clear trend in lateral diffusion was found due to unsaturation, the analysis of the autocorrelation functions of intramolecular vectors revealed that the rotational dynamics increase due to unsaturation. This increase was found essentially in every part of the molecules. The interfacial vector between the first carbons of the fatty acyl chains is the most slowly rotating vector in these molecules, describing the rotational motion of the whole molecule. This vector was found to lie, on average, parallel to the membrane surface. The rotational motion of C−H bonds was found to increase strongly along the chains toward the methyl end. The increase is most prominent in the next carbons from the double bonds toward the methyl end. This is most likely related to the recently found extraordinary flexibility of the single bonds in the neighborhood of double bonds; in the case of a chain containing six double bonds, the flexibility becomes more prominent toward the ends of the chains.

When it comes to the lateral pressure profiles in the simulated systems, it can be first concluded that we were able to reproduce the main features of the profile for saturated DPPC, in agreement with earlier molecular dynamics simulation studies.[46,48,87] Interestingly, there was a shallow peak of pressure in the middle of the DPPC bilayer, which, however, disappeared gradually in POPC, PLPC, PAPC, and PDPC bilayers. This peak has also been observed in other atomic-scale computational studies for DPPC and in the theoretical model of Mukhin and Baoukina.[93] The experiment conducted by Templer et al.[89] also suggests the existence of the peak. We could ensure from the simulation data that the disappearance of the peak in the membrane center was not related to changes in the interdigitation of the acyl chains, which was earlier suggested to explain the emergence of the peak in the interior of a DPPC bilayer.[91] Alternatively, Gawrisch and Holte[92] have suggested that decrease in the order of the hydrocarbon chains would be related to an increase in the lateral pressure profile. This would not, however, directly explain the disappearance of the central pressure peak, as in the middle of all of the bilayers the order parameters are almost zero. Though, ordering could explain the change in the central region indirectly, as due to unsaturation there appears to be a strong decrease of ordering toward the glycerol region of the chains. It is plausible that this would lead to an increase in the area per lipid, which would, in turn, lead to a conclusion that the lateral pressure in the middle of the bilayer is decreased due to polyunsaturation.

Overall, the results are in line with previous suggestions of the effects of membrane composition on, e.g., lipid−rhodopsin interactions[18−20] and the gating of mechanosensitive channels such as MscL.[13,91] Both ideas are essentially based on the concept of the lateral pressure profile. Interestingly, it was formulated already approximately two decades ago in terms of spontaneous curvature and curvature stress in the context of rhodopsin−lipid interactions.[18−20] The present work has shown that the lateral pressure profile indeed depends rather strongly on the unsaturation level of the lipid matrix. The role of the lateral pressure profile has also been discussed in relation to the mechanism of general anesthesia, which has been an open question for a long time in the field of membrane biophysics. In the late 1990s, Robert Cantor presented a simple model suggesting that incorporation of amphiphilic or other interfacially active solutes into the bilayer increases the interfacial lateral pressure, which then results in the decreased lateral pressure in the center of the bilayer. In case of ion channels, this redistribution of lateral pressure would cause a shift of the protein conformational equilibrium toward a closed state, resulting in a possible mechanism for general anesthesia.[15]

Summarizing, including the present data, there now seems to be a reasonable amount of evidence suggesting that the molecular composition of membranes affects the lateral pressure profile[17,46−48,87] exerted on membrane proteins. This would affect its structure and hence its activity. However, due to the lack of complete studies of lateral pressure profiles in the presence of membrane proteins, this intriguing hypothesis remains to be fully validated.

Acknowledgment. We thank Jarmila Repáková for providing the simulation trajectory of the DPPC system, Arvi Rauk and Michal Bachar for correspondence, and Perttu Niemelä for fruitful discussions. This work has, in part, been supported by the Academy of Finland (M.T.H. and I.V.), the Academy of Finland Center of Excellence Program (S.O. and I.V.), and the Jenny and Antti Wihuri Foundation (M.T.H.). We further acknowledge the Finnish IT Center for Science and the HorseShoe (DCSC) supercluster computing facility at the University of Southern Denmark for computer resources.

Supporting Information Available: Additional plot to illustrate the original raw data (prior to spline-based smoothing) for the lateral pressure profiles presented in the article. This material is available free of charge via the Internet at http://pubs.acs.org.

References and Notes

(1) Hooper, L.; Thompson, R. L.; Harrison, R. A.; Summerbell, C. D.; Ness, A. R.; Moore, H. J.; Worthington, H. V.; Durrington, P. N.; Higgins, J. P. T.; Capps, N. E.; Riemersma, R. A.; Ebrahim, S. B. J.; Smith, G. D. *BMJ* **2006**, *332*, 752−760.

(2) Feller, S. E.; Gawrisch, K. *Curr. Opin. Struct. Biol.* **2005**, *15*, 416−422.

(3) Stillwell, W.; Wassall, S. R. *Chem. Phys. Lipids* **2003**, *126*, 1−27.

(4) Eldho, N. V.; Feller, S. E.; Tristram-Nagle, S.; Polozov, I. V.; Gawrisch, K. *J. Am. Chem. Soc.* **2003**, *125*, 6409−6421.

(5) Mihailescu, M.; Gawrisch, K. *Biophys. J.* **2006**, *90*, L04−L06.

(6) Wassall, S. R.; Brzustowicz, M. R.; Shaikh, S. R.; Cherezov, V.; Caffrey, M.; Stillwell, W. *Chem. Phys. Lipids* **2004**, *132*, 79−88.

(7) Gawrisch, K.; Eldho, N. V.; Holte, L. L. *Lipids* **2003**, *38*, 445−452.

(8) Seelig, A.; Seelig, J. *Biochemistry* **1977**, *16*, 45−50.

(9) Hyvönen, M. T.; Ala-Korpela, M.; Vaara, J.; Rantala, T. T.; Jokisaari, J. *Chem. Phys. Lett.* **1995**, *246*, 300−306.

(10) Salmon, A.; Dodd, S. W.; Williams, G. D.; Beach, J. M.; Brown, M. F. *J. Am. Chem. Soc.* **1987**, *109*, 2600−2609.

(11) Hyvönen, M. T.; Kovanen, P. T. *Eur. Biophys. J.* **2005**, *34*, 294−305.

(12) Safran, S. A. *Statistical Thermodynamics of Surfaces, Interfaces, and Membranes*; Addison-Wesley: Reading, MA, 1994.

(13) Cantor, R. S. *J. Phys. Chem. B* **1997**, *101*, 1723−1725.

(14) Cantor, R. S. *Biophys. J.* **1999**, *76*, 2625−2639.

(15) Cantor, R. S. *Biochemistry* **1997**, *36*, 2339−2344.

(16) Kuiper, M. Azobenzene-Substituted Phosphate Amphiphiles. Ph.D. Thesis, Rijksuniversiteit Groningen, Groningen, The Netherlands, 2005.

(17) Carrillo-Tripp, M.; Feller, S. E. *Biochemistry* **2005**, *44*, 10164−10169.

(18) Wiedmann, T. S.; Pates, R. D.; Beach, J. M.; Salmon, A.; Brown, M. F. *Biochemistry* **1988**, *27*, 6469−6474.

(19) Gibson, N. J.; Brown, M. F. *Biochemistry* **1993**, *32*, 2438−2454.

(20) Brown, M. F. *Chem. Phys. Lipids* **1994**, *73*, 159−180.

(21) Bachar, M.; Brunelle, P.; Tieleman, D. P.; Rauk, A. *J. Phys. Chem. B* **2004**, *108*, 7170−7179.

(22) Tieleman, D. P.; Berendsen, H. J. C. *J. Chem. Phys.* **1996**, *105*, 4871−4880.

(23) Tieleman, D. P.; Berendsen, H. J. C. *Biophys. J.* **1998**, *74*, 2786−2801.

(24) Falck, E.; Patra, M.; Karttunen, M.; Hyvönen, M. T.; Vattulainen, I. *Biophys. J.* **2004**, *87*, 1076−1091.

(25) Patra, M.; Karttunen, M.; Hyvönen, M.; Falck, E.; Vattulainen, I. *J. Phys. Chem. B* **2004**, *108*, 4485−4494.
(26) Patra, M.; Karttunen, M.; Hyvönen, M. T.; Falck, E.; Lindqvist, P.; Vattulainen, I. *Biophys. J.* **2003**, *84*, 3636−3645.
(27) Niemelä, P.; Hyvönen, M.; Vattulainen, I. *Biophys. J.* **2004**, *87*, 2976−2989.
(28) Kupiainen, M.; Falck, E.; Ollila, S.; Niemelä, P.; Gurtovenko, A. A.; Hyvönen, M. T.; Patra, M.; Karttunen, M.; Vattulainen, I. *J. Comput. Theor. Nanosci.* **2005**, *2*, 401−413.
(29) Repáková, J.; Čapková, P.; Holopainen, J. M.; Vattulainen, I. *J. Phys. Chem. B* **2004**, *108*, 13438−13448.
(30) Repáková, J.; Holopainen, J. M.; Morrow, M. R.; McDonald, M. C.; Čapkova, P.; Vattulainen, I. *Biophys. J.* **2005**, *88*, 3398−3410.
(31) Patra, M.; Salonen, E.; Terämä, E.; Vattulainen, I.; Faller, R.; Lee, B. W.; Holopainen, J.; Karttunen, M. *Biophys. J.* **2006**, *90*, 1121−1135.
(32) der Spoel, D. V.; Lindahl, E.; Hess, B.; van Buuren, A. R.; Meulenhoff, E. A. P. J.; Tieleman, D. P.; Sijbers, A. L. T. M.; Feenstra, K. A.; van Drunen, R.; Berendsen, H. J. C. *GROMACS User Manual*, version 3.2.; 2004.
(33) Berendsen, H. J. C.; van der Spoel, D.; van Drunen, R. *Comput. Phys. Commun.* **1995**, *91*, 43−56.
(34) Lindahl, E.; Edholm, O. *Biophys. J.* **2000**, *79*, 426−433.
(35) Berendsen, H. J. C.; Postma, J. P. M.; van Gunsteren, W. F.; DiNola, A.; Haak, J. R. *J. Chem. Phys.* **1984**, *81*, 3684−3690.
(36) Hoover, W. G. *Phys. Rev. A* **1985**, *31*, 1695−1697.
(37) Nosé, S. *Mol. Phys.* **1984**, *52*, 255−268.
(38) Nosé, S.; Klein, M. *Mol. Phys.* **1983**, *50*, 1055−1076.
(39) Parrinello, M.; Rahman, A. *J. Appl. Phys.* **1981**, *52*, 7182−7190.
(40) Essman, U. L.; Perera, M. L.; Berkowitz, M. L.; Larden, T.; Lee, H.; Pedersen, L. G. *J. Chem. Phys.* **1995**, *103*, 8577−8592.
(41) Hess, B.; Bekker, H.; Berendsen, H. J. C.; Fraaije, J. G. E. M. *J. Comput. Chem.* **1997**, *18*, 1463−1472.
(42) Miyamoto, S.; Kollman, P. A. *J. Comput. Chem.* **1992**, *13*, 952−962.
(43) Berendsen, H. J. C.; Postma, J. P. M.; van Gunsteren, W. F.; Hermans, J. In *Intermolecular Forces*; Pullman, B., Ed.; Reidel: Dordrecht, The Netherlands, 1981; pp 331−342.
(44) Schofield, P.; Henderson, J. R. *Proc. R. Soc. London, Ser. A* **1982**, *379*, 231−246.
(45) Goetz, R.; Lipowsky, R. *J. Chem. Phys.* **1998**, *108*, 7397−7409.
(46) Lindahl, E.; Edholm, O. *J. Chem. Phys.* **2000**, *113*, 3882−3893.
(47) Gullingsrud, J.; Schulten, K. *Biophys. J.* **2004**, *86*, 3496−3509.
(48) Sonne, J.; Hansen, F. Y.; Peters, G. H. *J. Chem. Phys.* **2005**, *122*, 124903.
(49) Kirkwood, J. G.; Buff, F. P. J. *J. Chem. Phys.* **1949**, *17*, 338−343.
(50) Irving, J. H.; Kirkwood, J. G. *J. Chem. Phys.* **1950**, *18*, 817−829.
(51) Morante, S.; Rossi, G. C.; Testa, M. *J. Chem. Phys.* **2006**, *125*, 034101.
(52) Harasima, A. *Adv. Chem. Phys.* **1958**, *1*, 203−237.
(53) Nagle, J. F.; Tristram-Nagle, S. *Biochem. Biophys. Acta* **2000**, *1469*, 159−195.
(54) Kučerka, N.; Tristam-Nagle, S.; Nagle, J. F. *J. Membr. Biol.* **2005**, *208*, 193−202.
(55) Ghosh, D.; Tinoco, J. *Biochim. Biophys. Acta* **1972**, *266*, 41−49.
(56) Brockman, H. L.; Applegate, K. R.; Momsen, M. M.; King, W. C.; Glomset, J. A. *Biophys. J.* **2003**, *85*, 2384−2396.
(57) Rajamoorthi, K.; Petrache, H. I.; McIntosh, T. J.; Brown, M. F. *J. Am. Chem. Soc.* **2005**, *127*, 1576−1588.
(58) Brodnitz, M. H. *J. Agric. Food Chem.* **1968**, *16*, 994−999.
(59) Mitchell, D. C.; Litman, B. J. *Biophys. J.* **1998**, *74*, 879−891.
(60) Akutsu, H.; Nagamori, T. *Biochemistry* **1991**, *30*, 4510−4516.
(61) van Langen, H.; van Ginkel, G.; Shawn, D.; Levine, Y. K. *Eur. Biophys. J.* **1989**, *17*, 37−48.
(62) Stubbs, C. D.; Kouyama, T.; Kinosita, K.; Ikegami, A. *Biochemistry* **1981**, *20*, 4257−4262.
(63) Holte, L. L.; Peter, S. A.; Sinnwell, T. M.; Gawrisch, K. *Biophys. J.* **1995**, *68*, 2396−2403.
(64) Baenziger, J. E.; Jarrel, H. C.; Hill, R. J.; Smith, I. C. P. *Biochemistry* **1991**, *30*, 894−903.
(65) Drobnies, A. E.; van der Ende, B.; Thewalt, J. L.; Cornell, R. B. *Biochemistry* **1999**, *38*, 15606−15614.
(66) Petrache, H. I.; Salmon, A.; Brown, M. F. *J. Am. Chem. Soc.* **2001**, *123*, 12611−12622.
(67) Huber, T.; Rajamoorthi, K.; Kurze, V. F.; Beyer, K.; Brown, M. F. *J. Am. Chem. Soc.* **2002**, *124*, 298−309.
(68) Mendelsohn, R.; Davies, M. A.; Schuster, H. F.; Xu, Z.; Bittman, R. *Biochemistry* **1991**, *30*, 8558−8563.
(69) Vattulainen, I.; Mouritsen, O. G. In *Diffusion in Condensed Matter: Methods, Materials, Models*; Heitjans, P., Karger, J., Eds.; Springer: Berlin, 2004.
(70) Lindblom, G.; Orädd, G.; Filippov, A. *Chem. Phys. Lipids* **2006**, *141*, 179−184.
(71) Filippov, A.; Orädd, G.; Lindblom, G. *Biophys. J.* **2003**, *84*, 3079−3086.
(72) Vaz, W. L. C.; Clegg, R. M.; Hallmann, D. *Biochemistry* **1985**, *24*, 781−786.
(73) Ladha, S.; Mackie, A. R.; Harvey, L. J.; Clark, D. C.; Lea, E. J. A.; Brullemans, M.; Duclohier, H. *Biophys. J.* **1996**, *71*, 1364−1373.
(74) Dustman, J. M.; Casas, R. S.; Scheidt, H. A.; Eldho, N. V.; Teague, W. E.; Gawrisch, K. *Biophys. J.* **2005**, *88*, 27a.
(75) Niemelä, P.; Hyvönen, M. T.; Vattulainen, I. *Biophys. J.* **2006**, *90*, 851−863.
(76) Lindahl, E.; Edholm, O. *J. Chem. Phys.* **2001**, *115*, 4938−4950.
(77) Wohlert, J.; Edholm, O. *J. Chem. Phys.* **2006**, *125*, 204703.
(78) Brown, M. F.; Seelig, J.; Häberlen, U. *J. Chem. Phys.* **1979**, *70*, 5045−5053.
(79) Baenziger, J. E.; Jarrel, H. C.; Smith, I. C. P. *Biochemistry* **1992**, *31*, 3377−3385.
(80) Brown, M. F. *J. Chem. Phys.* **1984**, *80*, 2808−2831.
(81) Feller, S. E.; Gawrisch, K.; MacKerell, A. D., Jr. *J. Am. Chem. Soc.* **2002**, *124*, 318−326.
(82) Hyvönen, M. T.; Rantala, T. T.; Ala-Korpela, M. *Biophys. J.* **1997**, *73*, 2907−2923.
(83) Israelachvili, J. N. *Intermolecular and Surface Forces*; Academic Press: London, 1985.
(84) Israelachvili, J. N.; Marcelja, S.; Horn, R. G. *Q. Rev. Biophys.* **1980**, *13*, 121−200.
(85) Marsh, D. *Biochim. Biophys. Acta* **1996**, *1286*, 183−223.
(86) Seddon, J. M.; Templer, R. H. In *Structure and Dynamics of Membranes*; Lipowsky, R., Sackmann, E., Eds.; Elsevier: Amsterdam, 1995; pp 97−160.
(87) Patra, M. *Eur. Biophys. J.* **2005**, *35*, 79−88.
(88) Venturoli, M.; Smit, B. *Phys. Chem. Commun.* **1999**, *2*, 45−49.
(89) Templer, R. H.; Castle, S. J.; Curran, A. R.; Rumbles, G.; Klug, D. R. *Faraday Discuss.* **1998**, *11*, 41−53.
(90) Thijsse, B. J.; Hollanders, M. A.; Hendrikse, J. *Comput. Phys.* **1998**, *12*, 393−399.
(91) van den Brink-van der Laan, E.; Killian, J. A.; Kruijff, B. *Biochim. Biophys. Acta* **2004**, *1666*, 275−288.
(92) Gawrisch, K.; Holte, L. L. *Chem. Phys. Lipids* **1996**, *81*, 105−116.
(93) Mukhin, S. I.; Baoukina, S. *Phys. Rev. E* **2005**, *71*, 061918−061923.
(94) Litman, B. J.; Mitchell, D. C. *Lipids* **1996**, *31*, S193−S197.
(95) Attwood, P. V.; Gutfreund, H. *FEBS Lett.* **1980**, *119*, 323−326.
(96) Sakmar, T. P.; Menon, S. T.; Marin, E. P.; Awad, E. S. *Annu. Rev. Biophys. Biomol. Struct.* **2002**, *31*, 443−484.
(97) Ollila, S.; Rog, T.; Karttunen, M.; Vattulainen, I. *J. Struct. Biol.*, in press.
(98) Petrache, H. I.; Dodd, S. W.; Brown, M. F. *Biophys. J.* **2000**, *79*, 3172−3192.
(99) Seelig, J.; Waespe-Sarcevic, N. *Biochemistry* **1978**, *17*, 3310−3315.
(100) Rajamoorthi, K.; Brown, M. F. *Biochemistry* **1991**, *30*, 4204−4212.